

Limits on the Boron Isotopic Ratio in HD 76932

Luisa Rebull¹, Douglas Duncan¹, Sveneric Johansson², Julie Thorburn^{1,3}, & Brian Fields⁴

ABSTRACT

Data in the $\lambda 2090$ B region of HD 76932 have been obtained at high S/N using the HST GHRS echelle at a resolution of 90,000. This wavelength region has been previously identified as a likely candidate for observing the $^{11}\text{B}/^{10}\text{B}$ isotopic splitting.

The observations do not match a calculated line profile extremely well at any abundance for any isotopic ratio. If the B abundance previously determined from observations at $\lambda 2500$ is assumed, the calculated line profile is too weak, indicating a possible blending line. Assuming that the absorption at $\lambda 2090$ is entirely due to boron, the best-fit total B abundance is higher than but consistent with that obtained at $\lambda 2500$, and the best-fit isotopic ratio ($^{11}\text{B}/^{10}\text{B}$) is in the range $\sim 10:1$ to $\sim 4:1$. If the absorption is not entirely due to B and there is an unknown blend, the best-fit isotopic ratio may be closer to 1:1. Future observations of a similar metal-poor star known to have unusually low B should allow us to distinguish between these two possibilities. The constraints that can be placed on the isotopic ratio based on comparisons with similar observations of HD 102870 and HD 61421 (Procyon) are also discussed.

1. Introduction

Light element abundances in stars have much to tell us about big bang nucleosynthesis (BBN) and galactic chemical evolution. Only D, He, and ^7Li are predicted to be created in standard BBN (e.g. Wagoner, Fowler, & Hoyle 1967; Copi, Schramm, & Turner 1995); thus, observations of these elements can provide a check on BBN. Li, Be, and B (LiBeB) abundances increase with metallicity, and it is thought that the observed production is the result primarily of cosmic ray (CR) spallation. Since Meneguzzi, Audouze, & Reeves (1971), it has been thought that the reaction of fast protons and α particles on interstellar CNO is largely responsible for the creation of ^6Li , ^7Li , ^9Be , ^{10}B , and ^{11}B ; our recent work on the evolution of boron (Duncan *et al.* 1997, 1998) suggests that this canonical model is incomplete, and that the reverse process of spallation of heavier nuclei onto protons and α particles may be more important (see below). Additionally,

¹Department of Astronomy and Astrophysics, University of Chicago (rebull, duncan@oddjob.uchicago.edu)

²Department of Physics and Lund Observatory, Lund University, Sweden (SPEK_SEJ@garbo.lucas.lu.se)

³Yerkes Observatory, University of Chicago (thorburn@hale.yerkes.uchicago.edu)

⁴School of Physics and Astronomy, University of Minnesota (fields@mnhepw.hep.umn.edu)

simple CR spallation under-produces B (and Be) at low metallicities and predicts that $^{11}\text{B}/^{10}\text{B} \sim 2.5$, but the observed value in meteorites is 4.05 ± 0.2 (Chaussidon & Robert 1995). The ratio as observed in the interstellar medium (ISM) is 3.4 ± 0.7 (Lambert *et al.* 1998).

Because solving the B isotope problem must happen in the context of solving the total B evolution with metallicity, it is difficult to solve the B isotope problem without under- or over-producing the other light elements. One of the proposed solutions involves a large low-energy cosmic ray (LECR) component (of fast C,O) which spalls off protons and α particles in the ISM, and produces ^{11}B in sufficient quantity as to raise the predicted isotopic ratio (Ramaty *et al.* 1997; Vangioni-Flam *et al.* 1996). Woosley *et al.* (1990) have proposed that neutrino-induced nucleosynthesis in supernovae might produce measurable amounts of ^{11}B but essentially no ^{10}B , so as to increase the isotopic ratio. (This method also produces small amounts of ^7Li , as well as certain other species.) The production by neutrinos solves the boron isotopic problem, but the ν -process yields are very sensitive to the poorly constrained neutrino temperatures (and hence spectra); when incorporating its yields, one must be careful to produce enough ^{11}B to change the isotopic ratio to match meteoritic amounts, but at the same time, not overproduce B to the extent that the observed B/Be ratio is not fit. Several proposals have also been made regarding the destruction of one B isotope but not the other, but these seem unlikely. For modeling the evolution of the light elements, the boron isotopic ratio is the least constrained of all the light element data, and any additional information will help distinguish between models with various production and destruction mechanisms.

Johansson, Litzen, Kasten, and Kock (1993) measured in the lab the isotopic splitting of $^{11}\text{B}/^{10}\text{B}$ at $\lambda 2089.5$ to be $25 \text{ m}\text{\AA}$, corresponding to a resolution of about 85,000. Using the HST/GHRS echelle (nominal resolution $\sim 90,000$), we have observed the $\lambda 2090$ region of HD 76932 ($[\text{Fe}/\text{H}]=-1.0$). We will show that a clear result is not possible at this time. The data admit both the possibility that the feature at 2089.5 \AA is entirely due to B, and also the possibility that the feature is a blend of B and an unknown line. The resulting best-fit isotopic ratio in the two cases is different. The constraints that can be placed on the ratio are discussed, as well as a future observation which could distinguish between the two possibilities.

2. Observations and Data Processing

The *Hubble Space Telescope* (HST) *Goddard High-Resolution Spectrograph* (GHRS) was used in echelle mode ($R \sim 90,000$) to observe the B I $\lambda 2090$ region in HD 76932 on 3 October 1995. A total exposure time of 5.481 hours was obtained in 9 orbits. Due to the spacecraft losing lock on some of the observations, the resultant count rate in some exposures was low; the final S/N (per point) of the combined spectrum is ~ 55 . The total wavelength coverage is $2083.8-2094.8 \text{ \AA}$.

The point-spread function (PSF) of the HST/GHRS is comparable to the width of a diode (1 diode = $0.096-0.087 \text{ \AA}$; STScI 1995). Data was taken using standard observing strategies to

compensate for photocathode granularity, and to oversample the spectra such that the array of 500 diodes can be used as an array of effectively 2000 pixels. Thus, each point is not truly independent; a given diode affects the data recorded in 4 points. However, fourteen points define one wing of the $\lambda 2090$ boron line used for this work, and the S/N given above is per point, not per diode.

The data were processed using standard IRAF/STSDAS processing algorithms, the most significant of which are POFFSETS, which determines the relative shifts of the spectra via cross-correlation, and SPECALIGN, which shifts spectra to align in wavelength space and then sums them. The POFFSETS calculations were done in three equal sections to provide a consistency check; the relative shift separately determined from the three sections are averaged to calculate a robust shift for the spectrum as a whole. Data from different orbits were combined, weighted by the average number of counts in the raw spectrum.

The boron line and the region around it were examined in several subsets of the data. The feature is quite similar in each data set, and there are no additional features added by any one set. An exception was visit 5, which was significantly noisier than the other visits and was not included in the final summation. There were no unusually large photocathode granularity features that fall near the line of interest.

3. Wavelength Accuracies

The measurement that is sought is very dependent on small wavelength shifts. We have investigated the accuracy limits of the wavelength scale, both relative and absolute, using calibration (emission lamp) as well as stellar spectra. Calibration spectra were compared with a Pt-Ne line list, and stellar spectra with a Kurucz model line list.

3.1. Relative Accuracies

On-board and processing software algorithms compensate for the HST orbital Doppler shift (corrected for in-flight, ~ 8 km/s), and the Earth's motion around the Sun (corrected for in software, ~ 30 km/s). The FP-SPLIT strategy minimizes the impact of thermal effects, changes in plate scale ($\lesssim 0.1\%$), and geomagnetic effects ($\lesssim 0.5$ diode widths).

The limits of wavelength uncertainty intrinsic to the POFFSETS (cross-correlation) process represent the limits of comparing the data against itself, independent of any external wavelengths attached to the data. The net error measured in this fashion represents the error expected from photon statistics (as they affect wavelengths), as well as thermal effects, geomagnetic effects, etc. between the sub-exposures.

The shifts as calculated by the POFFSETS routine for each of three equal sections in each

spectrum were examined. The mean uncertainty found this way is 0.274 ± 0.06 px ($=0.0014$ Å). The uncertainty in the position of the wavelengths expected from photon statistics alone is about 1 mÅ, comparable to the net POFFSETS accuracy, so other effects do not contribute significantly to this source of error.

The emission line profile has been determined by GHRs staff to be Gaussian with a full-width-at-half-max (FWHM) of ~ 1.1 diodes. The on-board Pt-Ne lamp has 3000 lines measured to ± 0.2 mÅ (Reader *et al.* 1990). These known lines were used to calibrate the instrument on the ground, and polynomials used to solve for the dispersion. The wavelength scale attached to the data that comes from STScI is based on that formula, not on any calibrations taken at the same time as the science data. For our data, we requested Pt-Ne calibration exposures at each new carousel setting.

The calibration lamp emission line positions in the vicinity of the B I $\lambda 2090$ feature as measured via Gaussian line-fitting were compared directly with the line positions as recorded in the Pt-Ne line list of Reader *et al.* (1990). Over nine lines in all calibration observations the largest shift between observations is 2.9 mÅ. Within each observation, the mean differences in positions average to 0.004 ± 0.0015 Å. This error is a result of errors in the measurement of the Pt-Ne lines in the lab, errors in the polynomial fit to the known Pt lines that results in the wavelength file generated by STScI, and errors in carousel repeatability and wavelength dispersion. The overall mean offset of 4 mÅ likely represents a small systematic in carousel position calibration. The scatter in this offset, 1.5 mÅ, represents the random error in the carousel position, and is comparable to the error from POFFSETS.

3.2. Comparison of model and star lines

Another way of determining the wavelength scale of the data is to compare the wavelengths of lines in the stellar data with known wavelengths; this is an external comparison of wavelength accuracies. A comparison was made with a best-fit Kurucz synthetic spectrum computed from a model with stellar parameters as previously determined from the $\lambda 2500$ region (Duncan *et al.* 1997): $[\text{Fe}/\text{H}] = -1.0$, $\log g = 4.0$, and $T_{\text{eff}} = 6000$ K. The synthesis is discussed in more detail in §5 below. The error calculated in this fashion results from uncertainties in the Kurucz line list (in missing or unknown blending lines), in the determination of radial velocity, and in the dispersion/wavelength registration of the data.

Direct cross-correlation of the data and the synthetic spectrum is not possible (or desirable), as there are too many mismatches between the spectra. Therefore comparison was made of all lines between 2083 and 2092 Å which appeared to be unblended. Line centers of 41 such lines were measured via Gaussian fits and compared with the line positions given in the Kurucz list. The B line was not included since the reference for the wavelengths was necessarily different than that used for the rest of the Kurucz lines. The mean offset and standard deviation of the mean

was calculated, and, since there were several lines that were clearly discrepant between the model and data, outliers that were more than 1σ away from the mean were dropped, leaving 28 lines. The mean offset of these remaining points was $-1.497 \pm 0.0035 \text{ \AA}$, or 214.9 km/s. The standard deviation about the mean is 3.5 m\AA , and the standard deviation of the mean is thus $3.5/\sqrt{27}=0.7 \text{ m\AA}$. We therefore expect the net error of any given line to be the uncertainty of the measurement of the line itself (about 3.5 m\AA) and the uncertainty of the radial velocity determination for the entire spectrum (0.7 m\AA), added in quadrature, $\approx 3.5 \text{ m\AA}$. Since the 3.5 m\AA uncertainty for the line itself was determined based on the Kurucz lines, this uncertainty strictly only applies to the other Kurucz lines. It is, however, an upper limit for the error on the Johansson *et al.* (1993) measurements of the B lines. As expected, the absolute wavelength error ($\sim 4 \text{ m\AA}$) is larger than the relative error ($\sim 1.5 \text{ m\AA}$).

3.3. Conclusions on wavelength accuracies

The 1.4 m\AA limits of POFSETS represent the accuracy limits of comparing the data with itself. This is independent of external wavelengths attached to the data, and represents the error expected from photon statistics, thermal effects, geomagnetic effects, etc. The error expected from photon statistics alone (in wavelength space) is about 1 m\AA , comparable to the error determined.

Comparing the wavelength calibration exposures to the laboratory Pt-Ne line list reveals errors in the polynomial that assigns GHRs wavelengths and in grating carousel repeatability. The overall mean offset is 4 m\AA , and probably represents a systematic error in the polynomial used for assignment of wavelengths. Our best estimate of the random error in carousel placement is 1.5 m\AA . This error also represents an internal error, e.g. relative, not absolute, wavelength errors.

By comparing stellar lines to the lines in the Kurucz model, the absolute wavelength registration is recovered to an accuracy of at least 3.5 m\AA . As expected, the error in the absolute wavelengths is larger than that for the relative wavelengths. This error incorporates uncertainties in the Kurucz line list, in unknown blending lines, in the determination of radial velocity, and in the dispersion/wavelength registration of the data.

All sources of error investigated here are significantly less than the 25 m\AA isotopic splitting of boron.

4. PSF Considerations

Calibration as well as data files were used to probe the shape of the point-spread function (PSF). The PSF of the emission lines in the wavelength calibrations, although thermally broadened due to the temperature of the lamp, is still narrower than any stellar line obtained here. The mean FWHM of a Gaussian fit to a mean emission line is $\sim 0.025 \text{ \AA}$.

In the stellar data, the width of the lines is a combination of instrumental plus stellar broadening. The stellar broadening has components from rotation, macro- and microturbulence, and thermal motion of the atoms. In extremely high S/N data, it is possible to separately discern the contribution from some of these components, but in the present case only the net broadening is detectable from the data alone. IRAF was used to determine the widths and centers of Gaussians fit to more than 20 stellar lines. Many proved to be blended, and in order to determine the true broadening the narrowest and least blended lines were selected. The three narrowest stellar lines all had a FWHM of $0.0330 \text{ \AA} = \Delta v = 4.7 \text{ km/s}$.

Nissen *et al.* (1994), in determining the ${}^6\text{Li}/{}^7\text{Li}$ ratio in this star, derived a net FWHM of a radial-tangential profile fit of 4.7 km/s, exactly the same as the width determined here, despite the use of a different profile. The radial-tangential profile is designed to incorporate radial and tangential motions in the atmosphere; see Gray (1992). Nissen *et al.* (1994) used this profile because they detected a slight asymmetry in the red wing of the Li line, and they determined that this profile was a better fit than either a pure Gaussian or the standard rotational profile. Our data is not high enough S/N for such detailed comparisons.

For direct comparison to the B I feature, relatively isolated lines of comparable depth were needed. The narrowest stellar line found for this comparison was a line at 2091.4 \AA which is not included in the Kurucz list. Gaussians were fit to this line and the B feature. The width (σ) in \AA of the Gaussian fit to the narrow stellar line is 0.017, but the width of the boron line is 0.032 (see Figure 1 and further discussion below). It is clear that the boron line is much wider than the narrowest stellar lines. Since boron is a light nucleus, some additional broadening is expected from thermal motion of the atoms. The other identified lines near the B line are nearly all Fe or Al; B is a factor of about 5 and 2 lighter, respectively, thus, thermal effects are expected to widen the line by a factor of about $\sqrt{5}$ and $\sqrt{2}$, assuming that this unknown line is, in fact, Fe or Al. However, formal calculations are preferable, and the Kurucz synthesis incorporates thermal motion properly.

The boron line as detected here is quite symmetric, as are other lines in the spectrum. A simple way of determining the extent of the broadening and symmetry is to fit a Gaussian to the line and compare the data to the fit; regardless of the fact that the line is not truly described by a Gaussian, if it is symmetric, deviations from Gaussianity should also be symmetric. Figure 1a compares a Gaussian fit to the boron line, and Figure 1b does the same for the stellar line at 2091.4 \AA . Wings of adjacent features can be seen on the right. Residuals are also shown in each Figure. Conventions introduced in these Figures are used through the rest of this work. First, for reference and ease of comparison, (dotted) vertical lines delineating twice the width of the Gaussian are superimposed on the Figure as an approximate definition of the region dominated by the line in question. Second, data points are indicated by error bars delimiting photon statistics in the flux direction, and indicating true wavelength uncertainties (§3.3) in the wavelength direction. In this Figure, note that the boron line deviates from the fit in a symmetric manner, perhaps even more symmetrically than the 2091.4 \AA stellar line. The red wing of the boron line is very slightly wider than the blue wing. It is not clear whether the symmetry is really symmetry of the stellar

lines, or an artifact of the relatively low S/N of this spectrum.

Extensive tests of Gaussian fits (single and multiple) to these lines were performed, but none changed the fundamental conclusion that the boron line is much wider than nearby narrow stellar features. Since line profiles are not strictly expected to be Gaussian and especially since lines in stellar atmospheres do not add as two Gaussians would, spectral synthesis is needed to make a better attempt at accounting for the flux in overlapping lines.

5. Spectral Synthesis

Spectral synthesis using the latest Kurucz model atmospheres was done using the SYNTHE program distributed by Kurucz (1993) on CD-ROM. This program assumes local thermodynamic equilibrium (LTE) in determining level populations and calculating the emergent spectrum. Scripts written by Steve Allen (UC Santa Cruz) were used to run the program on Unix SparcStations. The grid of model atmospheres was that released by Kurucz on CD-ROM #13, which included in its computation the blanketing of almost 60 million lines, both atomic and molecular.

5.1. Boron line parameters

Johansson *et al.* (1993) measured the wavelengths and *gf* values of the $\lambda 2090$ B feature, and these parameters are used in the current work and summarized in Table 1. The line at 2088.9 Å is too blended for abundance analysis; this work is concerned only with the lines at 2089.5 Å. The quoted error on wavelengths is 0.2 mÅ. The error on the *gf* values is estimated at 5–10%.

In careful work done previously with line shapes and isotopic splittings of Li, the hyperfine structure (hfs) of the splittings was important (Hobbs & Thorburn 1994). Johansson *et al.* (1993) state that the isotope and fine-structure splitting is much larger than the hfs, and therefore hfs is not a source of error here. Specifically in the case of Li, one must worry about where each isotope falls on a curve of growth, as one component will saturate at a different rate than the other, changing the shape of the line in ways that might appear to be caused by a different isotopic ratio. However, in the present case such errors are smaller than other errors here and are not considered.

5.2. Other lines

The initial line list used in the spectrum synthesis included the 577 Kurucz lab lines around $\lambda 2090$. There are more than 37 000 predicted lines, but as these predicted wavelengths can be wrong by several Å, predicted lines were not used in the detailed analysis. However, the addition of predicted lines is valid in a statistical sense, and their inclusion depresses the overall level of continuum ($\sim 0.5\%$). This is less than the other uncertainties in the normalization process.

Several published line lists were consulted for updates to the Kurucz line list, but no significant updates were obtained. Our line list is available upon request via email to rebull@oddjob.uchicago.edu.

We did not adjust the gf values for any of the lines, as we had insufficient stars to constrain the lines. Changing the gf values for lines close to 2089.5 Å (such as the one seen redward of the B line in the Figures) has no effect on the isotopic fits.

5.3. Previously determined model and initial fits

Our previous work at $\lambda 2500$ determined the best-fit Kurucz model for HD 76932 to have the parameters $[\text{Fe}/\text{H}]=-1.0$, $\log g=4.0$, $T_{\text{eff}}=6000$ (Duncan *et al.* 1997). Microturbulence, as in the previous work, was selected from the literature to be 2.0 km/s. The Kurucz synthesis treats macroturbulence as a Gaussian smoothing operation, and adds rotational broadening by disk integration. The net broadening determined above (§4) is 4.7 km/s, which was somewhat arbitrarily apportioned in the synthesis between macroturbulence and $v \sin i$, in the amounts 1.5 km/s for macroturbulence and 4.5 km/s for $v \sin i$. (i.e. we have used a standard value of 1.5 km/s for macroturbulence, c.f. Magain 1989.) Our S/N is not high enough to distinguish between these contributions.

The boron abundance reported in Duncan *et al.* (1997) was 1.82 ± 0.2 (in the usual notation $\log \epsilon(\text{B}) = 12.00 + \log \text{N}(\text{B})/\text{N}(\text{H})$). However, the gf values for the B I $\lambda 2090$ feature are known only from difficult laboratory measurements, and have not been constrained via observation in a wide range of stars. We therefore estimated another 10% uncertainty due to the $\lambda 2090$ gf values. This brings the effective uncertainty in boron abundance to ~ 0.25 dex.

Figure 2 includes the data and the synthetic spectrum fit; the net broadening is 4.7 km/s, the boron isotope ratio in the synthesis is 1:1, and the total boron abundance 1.82 dex. The boron lines are indicated at 2089.5 Å (the primary ones in this analysis) and 2088.9 Å (too blended to be of use here).

It can be seen in Figure 2 that the boron abundance of 1.82 does not provide a good fit to the B line. Increasing the boron abundance to 2.07 dex provides a much better fit. Note that this new abundance, while higher, is still consistent with the previous determination at $\lambda 2500$, within $\sim 1\sigma$.

6. Syntheses with Different Isotopic Ratios

Models were calculated for isotopic ratios ($^{11}\text{B}/^{10}\text{B}$) of 1:1, 2.5:1, 4:1, and 10:1, covering the range of galactic chemical evolution model predictions. As mentioned in §5.3 above, the lower boron abundance of 1.82 dex, derived from the B I 2500 Å line, does not provide a good fit to the data. Consequently, the synthesis profile does not match the data profile well at any isotopic ratio,

as seen in Figure 3. Either the boron abundance in the star is larger, or there is an unidentified line deepening the profile. The plot with total $\log \epsilon(\text{B})=1.82$ is included here for completeness because of the possibility that the abundance as derived from $\lambda 2500$ is correct and that there is another absorption line present; see §7. A synthetic profile that is much closer to the data can be calculated for a higher B abundance of 2.07 dex, which is within 1σ of and therefore consistent with the $\lambda 2500$ determination; this is shown in Figure 4a. Residuals from the total $\log \epsilon(\text{B})=2.07$ fit (data–model) are presented in Figure 4b. For each residual, as in previous Figures, the dotted vertical lines are for reference and appear at the same wavelengths in the plots of the line and the residuals. Within the region defined by these dotted lines, the mean and standard deviation of the residuals are indicated on the plot. The locations of the boron line components are also indicated with solid vertical lines between 2089.551 and 2089.590 Å.

Using this best-fit synthesis of $\log \epsilon(\text{B})=2.07$, and ignoring the possibility of a blending line, isotopic ratios of 1:1 and 2.5:1 appear to be ruled out, as they are too far offset to the red on both wings. Note that although the data and 10:1 or 4:1 synthesis line shapes agree relatively well on the blue wing, the shape of the red wing agrees less well and it is not clear whether the data are more appropriately fit by the 10:1 or 4:1 profiles. Deviations from the red wing are smaller for the 4:1 profile, but the 10:1 fit is better on the blue, and slightly better overall. Since the blue wing fits the shape of the profile reasonably well, it would be expected that the red wing would match to a comparable degree. However, in this fit, the red wings of the synthesis and data are distinctly different.

6.1. On the shape of the line and possible offsets

Interestingly, at this higher B abundance, the *shape* of the stellar line is quite well-matched to the synthesis line profile for a ratio of 1:1, although the *position* is not. In order to force the 1:1 profile to align with the data, a shift of $+0.007$ Å is required in addition to the radial velocity shift of -1.497 Å; see Figures 5a and b for such a shifted fit and residuals. Note that although the overall match with the shifted profile is quite good, the red wing is still the more discrepant. A similar kind of shift does not provide a good match at any other isotopic ratio, consistent with the observations in §4 that the line is very symmetric (other isotopic ratios produce less symmetric synthetic profiles).

Johansson *et al.* quote a wavelength accuracy of 0.2 mÅ for the B features, more than an order of magnitude less than 7 mÅ. However, since the wavelengths of the B features are necessarily coming from another source than the rest of the Kurucz lines, the possibility must at least be raised that the boron wavelengths from Johansson *et al.* and the rest of the wavelengths from Kurucz might be offset with respect to each other. However, an offset of as large as 7 mÅ seems extremely unlikely. No source of such an error was found.

The radial velocity associated with this 7 mÅ offset is $\sim 2\sigma$ away from the best-fit radial

velocity as determined in §3.2 above. At this new shift the other lines in the spectrum appear clearly offset with respect to the synthesis. Motions of on the order of 1 km/s would be required to create an offset of 7 mÅ. It is difficult to imagine a situation such that the parcel of gas responsible for the B absorption was moving away from the observer relative to the other lines in order to account for this offset. For more discussion on this subject, see the comparison with HD 102870 (§9) below.

Any systematic offset in Johansson *et al.* if present at $\lambda 2090$, might also be present at the $\lambda 2500$ B line they also measured. That spectral region has been more widely studied, and the results of Johansson *et al.* can be roughly compared with other authors (Morton *et al.* 1991; Edlén *et al.* 1970; Wagman 1937). In all cases, all the measurements are quite consistent with each other, especially since previous work has been done using (nonlinear) photographic plates, and the most recent work uses a Fourier Transform Spectrometer, estimated at an order of magnitude improved in quality. The comparison with other laboratory measurements thus gives no support to the possibility of an error in the lab wavelength as the source of a 7 mÅ shift as described above.

7. Syntheses with Different Isotopic Ratios and a Possible Blending Line

Until this point, we have assumed that the absorption at $\lambda 2090.5$ is largely due to boron. However, it is possible that there is an interloping absorption feature from an unknown species other than boron. An unknown line, if it is present, could be any of a wide range of strengths and locations. As an attempt at quantifying the impact of a blending absorption feature, a relatively weak line was selected from elsewhere in the spectrum to use as an artificial line for several test syntheses. The line selected was a neutral silicon line at 2086.747 ($\log gf = -4.275$), and in the synthetic spectrum (with broadening) it has a core intensity of about 0.4. This line was added to the line list at several locations in the boron profile, and the gf value adjusted as necessary.

Of the parameter space explored, the best fits were, for $\log \epsilon(\text{B})=1.82$, a blending line at 2089.560 Å, with a gf value of -3.875 (shown in Figure 6) and, for $\log \epsilon(\text{B})=2.07$, a blending line at 2089.575 Å, with the gf value of -4.275 (shown in Figure 7). As can be seen in the Figures, in the fits with the higher boron abundance, the 1:1 and 2.5:1 ratios continue to be ruled out, due to discrepancies on both the blue and the red wings. The fits with the lower boron abundance of $\log \epsilon(\text{B})=1.82$ and the bluer blending line match the line shape the least well on the red side, less well than the $\log \epsilon(\text{B})=2.07$ fits, although all models match the blue side fairly well. Unlike all of the other syntheses, however, these favor a 1:1 ratio and rule out the 10:1 ratio.

In conclusion, if there is a blending line near 2089.575 (or no blend at all), then the 1:1 and 2.5:1 isotopic ratios are ruled out. A blend at about 2089.560, however, allows these ratios. Making arguments solely on the shape of the PSF and the consistency with which the models can duplicate the line shape, it seems likely that any blend, if it exists, is near 2089.575. Thus, evidence is in favor of the higher B isotopic ratio, but a ratio of 1:1 can not be completely ruled

out. Based on these tests in particular, unambiguous conclusions about the boron isotopic ratio are not possible unless independent information on possible blends is known.

8. Additional Sources of Error

Some of the sources of error usually considered in synthesis fits are irrelevant here, because the S/N of the data is not extremely high, and because it is not clear whether or not there are unknown blending lines present. Here, the boron line is so deep that it is fortunately not particularly sensitive to the choice of normalization, and changes in normalization have no impact on our results. The microturbulence cannot be determined from this data, and thus the literature value of 2.0 km/s was used. The B line is not expected to be particularly sensitive to errors in $\log g$, and indeed, large changes in $\log g$ result in little change to the boron abundance (much smaller than other errors here) and in no change to the best-fit isotopic ratio.

The amount of flux the models predict for this region is sensitive to the metallicity and T_{eff} selected. A realistic uncertainty on the metallicity is ± 0.1 dex, and the subsequent effect on the boron abundance is less than 0.1 dex. In terms of the best-fit isotopic ratio, a more metal-poor model does not fit any of the profiles well due to a mismatch on the red wing; for a more metal-rich model, there is a preference for the 10:1 profile. A realistic error on T_{eff} is ± 75 K; similarly, the boron abundance is changed by less than 0.1 dex. The hotter model required slightly more boron to fit the data, but did not result in a change in the best-fit isotope profile. The cooler model did not require much change in boron abundance, and fit the 10:1 profile better than the 4:1 profile.

The net error in boron abundance on this determination is at minimum comparable to that quoted from the $\lambda 2500$ determination, ± 0.20 dex. A good guess for an uncertainty on this result is ± 0.25 dex. The errors in stellar parameters do not have a significant effect on the isotopic ratio; in general, if they suggest a change at all, they are more consistent with the higher isotopic ratios.

8.1. NLTE implications

Duncan *et al.* (1997) used the NLTE corrections of Kiselman & Carlsson (1996). The NLTE correction for abundances determined at either $\lambda 2500$ or $\lambda 2090$ increase the abundance determined using LTE methods. The $\lambda 2090$ correction is 0.35, and that of $\lambda 2500$ is 0.17. Although the LTE determinations of the B abundance in this star at the two wavelengths are consistent to within the standard error of measurement, using these NLTE corrections causes the discrepancy between the abundance determination to increase. If the changes suggested by the NLTE calculations are correct, then the two abundance determinations are no longer consistent to within a $1-\sigma$ error, and such a difference is thus harder to explain by statistical fluctuations. This may be taken as weak evidence that there is an unknown blending line affecting the $\lambda 2090$ feature. However, NLTE calculations can place no further constraints on the presence of a blending line.

9. Data for Other Stars: HD 102870 and HD 61421

We observed HD 102870 as part of this proposal, and data exists in the HST archive for HD 61421 (Procyon).

The stellar parameters of HD 102870 as determined from the literature are $[\text{Fe}/\text{H}]=+0.2$, $\log g=4.2$, $T_{\text{eff}}=6100$. The total exposure time for the HD 102870 data was 59.84 minutes; the resultant S/N per pixel is ~ 35 . The data for HD 61421 (Procyon) are very high S/N, since it is a very bright star. Total exposure time is 34.28 minutes. Literature values for Procyon are approximately $[\text{Fe}/\text{H}]=+0.03$, $\log g=4.0$, and $T_{\text{eff}}=6500$. In Figure 8, the HD 102870 data are seen as the thin line and HD 61421 is seen as the dotted line. Data from both stars were scaled for comparison to the HD 76932 data. The synthetic spectra for the high-metallicity stars indicates a pseudo-continuum close to 0.4, rather than the value of ~ 0.9 seen in HD 76932. Many lines which are too weak to affect the HD 76932 synthesis affect these more metal-rich stars, causing the continuum placement to be very uncertain. Thus, direct analysis of the isotopic abundance in these metal-rich stars was not attempted. Instead, the continuum was scaled to allow the side-by-side comparisons shown in the figure.

In HD 102870, the B line is at a wavelength extremely consistent with that in HD 76932, to well within measurement errors at 0.3 mÅ. There is no additional relative shift here between the boron line and the rest of the lines in the spectrum. If some physical effect is invoked to explain the 7 mÅ shift, it must operate identically in HD 102870, a much more metal-rich star. Thus, convective motions do not seem to be the culprit for creating a 7 mÅ offset.

As can be seen in the Figure, there appears to be little boron in HD 61421. Lemke, Lambert, and Edvardsson (1993) studied the $\lambda 2500$ region of this star, and concluded that it was depleted in boron by a factor of at least three. This star is also highly depleted in Li and Be, so B depletion may be expected from stellar structure grounds. Note that there is little evidence of any possible blending feature at the wavelength of the B line. The most likely candidate for an unknown blending line is an Fe or Al line, but in this more metal-rich star, such a line should be seen. It is, of course, possible that the 500 K difference in temperatures could also be responsible for the line disappearing. However, even in the worst-case scenario of a neutral atomic line, the effects of metallicity will dominate over the effects of temperature, thus arguing in favor of no blending line. Several sample syntheses were run to confirm that 500 K is not sufficient to completely remove such a blending line. The facts that this star has no or little boron and the $\lambda 2090$ line nearly disappears are a strong argument for the absorption being largely due to B, with no unknown blending line.

Interestingly, the weak absorption line in the Procyon spectrum is located at 2089.548 Å, which is distinctly off-center from the B lines centered at 2089.571 Å. Several syntheses with an artificial line were run in the same vein as §7 above, with the artificial line at the position of this vestigial line. However, since this line is distinctly blueward of the B lines (22 mÅ), the changes in the syntheses are all on the blue wing of the line, not the more-problematic red side.

Observations of the $\lambda 2090$ region in stars closer in stellar parameters to HD 76932, preferably with known varying amounts of boron, could clarify the issue of whether or not there is a blending line. The B-poor halo stars, measured by Primas *et al.* (1998) would be ideal targets.

10. Discussion

The present work was undertaken to constrain galactic chemical evolution models. Since Reeves, Fowler, & Hoyle (1970), it has been known that Galactic cosmic rays (GCRs) are involved in the formation of light elements. However, the $^{11}\text{B}/^{10}\text{B}$ ratio predicted by the spallation of cosmic ray (CR) protons and α -particles off of C, N, and O in the ISM is 2.5; this is only marginally consistent with the meteoritic ratio known for some time to be near 4 (most recently 4.05 ± 0.2 , Chaussidon & Robert 1995), or the ISM ratio, recently determined to be 3.4 ± 0.7 (Lambert *et al.* 1998). Thus, an additional source of B is needed.

Three possible contributors to light element abundances in the Galaxy (besides BBN and AGB stars for Li) have been widely discussed recently. The mechanism described immediately above, Galactic cosmic ray (GCR) protons and α -particles spalling off of C, N, and O in the ISM, is the mechanism traditionally thought to make light elements in the Galaxy. A second process is the neutrino (ν) process originally suggested by Woosley *et al.* (1990) where ν 's created in the collapsing core of a massive supernova induce nuclear reactions in the outer metal-rich layers of the star. Yields of this process are very uncertain, because the ν temperature is poorly constrained by SN models. The last process most recently discussed is low-energy cosmic rays (LECRs), metal-rich material accelerated by massive stars and spalling off H and He in the ISM. This is a reverse of the traditional GCR spallation process. Models of this process show interesting results that seem to match the light element evolution; however, LECRs, while appearing promising, have an uncertain physical origin.

Vangioni-Flam *et al.* (1996; hereafter VCFO) developed models with all three of these components operating, and made specific predictions for, among other things, the $^{11}\text{B}/^{10}\text{B}$ ratio. The light elements produced by these processes are listed by isotope in Table 2 (based on a similar table in VCFO). Table 2 also contains rough predictions for $^{11}\text{B}/^{10}\text{B}$. Note that this prediction is often sensitive to the input parameters of the model, and that, if several processes are operating, the products must be mixed together in the ISM, effectively lowering high ratios and raising low ratios.

The LECR component is constrained by observations by instruments on the *Compton Gamma Ray Observatory*, both detections (Bloemen *et al.* 1994) and non-detections (Murphy *et al.* 1996). The astrophysical source is uncertain, so VCFO tried several different models and source compositions, all of which had spectra essentially flat up to a cutoff energy ~ 30 MeV. Regardless of variations in the models, the LECR component as modelled by VCFO seems able to account for adequate Be in the early Galaxy as well as the approximately linear Be and B evolution

with metallicity seen in the data. The ν -process, however, only produces selected isotopes, and thus the yields of this process must be carefully tuned to maintain agreement with observations of the other light elements. Future observations of other ν -process products like fluorine might provide additional constraints. Since the ν energy and spectrum are quite uncertain, this tuning is relatively unconstrained; VCFO tuned the yields to match the meteoritic $^{11}\text{B}/^{10}\text{B}$. The rest of the VCFO models also converge to the single data point at solar metallicity; the current study is of course working at a metallicity of ~ -1 . If one takes the results of this work to be that $^{11}\text{B}/^{10}\text{B} \sim 4-10$, with a slight preference for the higher value, then this work is consistent with all of the VCFO predictions. If the results of this work are taken to be that the isotopic ratio is low, closer to 1:1, then none of these specific models are consistent.

Ramaty *et al.* (1997; hereafter RKLR) make specific predictions about the $^{11}\text{B}/^{10}\text{B}$ ratio. Working with the three basic processes listed above, they adjust the energy spectrum and elemental composition of the LECR using, for example, ejecta specified by models of massive SNe and WR stars. They investigate a different parameter space than VCFO, taking into account one-step processes that create LiBeB immediately, as well as two-step processes that result in LiBeB through an intermediate nucleus, over a wide range in energies. RKLR claim that, since GCR under-produces the isotopic ratio, and LECR (regardless of specifics) tends to over-produce it, the two processes operating together provide an easy way to account for the meteoritic ratio, but the ν process is still required. Since the $^{11}\text{B}/^{10}\text{B}$ ratio until now has not been measured in stars, RKLR predict that $^{11}\text{B}/^{10}\text{B}$ will be measured in low-metallicity stars to be essentially consistent with (and not less than) the meteoritic value of 4.05 ± 0.2 (Chaussidon & Robert 1995); at higher metallicities, they argue, the Type Ia SNe begin to contribute to the metallicity (and the cosmic ray flux) but not directly to the B abundance. They find that it is difficult for cosmic rays alone to create the meteoritic $^{11}\text{B}/^{10}\text{B}$ abundance, and that either an artificial spectrum is needed or ^{11}B production in (Type II) SNe is required throughout the life of the Galaxy. RKLR make the prediction that if $^{11}\text{B}/^{10}\text{B} > 4$, then B/Be cannot be lower than ~ 16 , and if it is > 4 , then the B/Be and isotope ratios will be inconsistent. Similarly based on B/Be observations, they also predict that $^{11}\text{B}/^{10}\text{B} < 7$. Taking the results of the present investigation to be that $^{11}\text{B}/^{10}\text{B} \sim 4-10$, with a slight preference for the higher value, our work is consistent with this prediction. Similarly, a lower isotopic ratio of 1:1 is not consistent with the predictions.

Unfortunately, the relatively wide ratio admitted by present data do not sharply constrain models. Observations of the isotope ratio in more metal-poor stars (assuming constraints on blending lines obtained from stars similar in parameters to HD 76932 but B-weak) would better distinguish between these models.

11. Conclusions

Assuming that the line feature observed at 2090 \AA is composed solely of absorption due to B, then the boron abundance determined here is $\log \epsilon(\text{B}) = 2.07$, which is within 1σ of the boron

abundance determined at $\lambda 2500$, 1.82. In this case, low $^{11}\text{B}/^{10}\text{B}$ isotope ratios such as $\sim 1:1$ or $2.5:1$ are ruled out, and the data are most consistent with the higher ratios of $\sim 4:1$ or $10:1$.

However, the line shape, particularly the red wing, does not match the profiles from either a ratio of $4:1$ or $10:1$ particularly well. It happens to match the shape of the $1:1$ profile (both wings) quite well, but only if an ad-hoc shift of $7 \text{ m}\text{\AA}$ is introduced. This shift is an order of magnitude larger than the expected errors in the Johansson *et al.* laboratory B wavelengths, and we have not found any other reason for a shift. It cannot be due to a relative radial velocity shift between B and the other stellar lines, unless one arbitrarily introduces a shift $\sim 2\sigma$ away from the best-fit radial velocity determined from the lines in our spectrum other than B. Reasonable changes in stellar parameters are not able to create a better fit, although some selected parameter changes do favorably affect the profile shape. All changes investigated here suggest that the higher isotope ratios are correct; none suggest that the lower isotope ratios are correct. A simple examination of the NLTE corrections weakly suggest the presence of a blending line.

A blending line might simultaneously explain why the 2090 \AA B feature gives a higher abundance than the $\lambda 2500$ lines and why the profile-fitting was not more successful. In this part of the uv spectrum many stellar lines remain unidentified. Assuming that the true B abundance of this star is really 1.82, we have shown that if there was a blending line of the right strength near 2089.560 \AA , the isotopic ratio could be low. If the B abundance is really higher, closer to the 2.07 determined here, a blending line could still be present at 2089.575 \AA . This blending line does not change the derived isotopic ratio, but rather adjusts the red wing shape at the expense of the blue to be more consistent with the observed profile.

Data from this line region of Procyon (HD 61421) were retrieved from the HST archive in order to search for a possible blending line. Only a vestigial line is observed in Procyon (which is B-weak) at $\lambda 2090$. With only a 500 K temperature difference between these stars, it seems unlikely that a significant blend would be present in HD 76932 but absent in Procyon. Moreover, the central wavelength of the vestigial feature in Procyon is offset from the expected B wavelength by $\sim 20 \text{ m}\text{\AA}$, a large difference. Based on this comparison, we conclude that there is probably no interloping feature that disrupts the B feature in the cooler or more metal-poor stars. We also conclude that this feature in Procyon is probably not B. This conclusion could be made much stronger if a star without B and closer in temperature and metallicity to HD 76932 could be observed.

A $^{11}\text{B}/^{10}\text{B}$ ratio of 4-10 is consistent with essentially all of the theoretical predictions made by VCFO and RLKR, which incorporate mixes of products of 3 processes, GCR spallation, ν -process, and LECRs. It is inconsistent with a pure GCR origin of B. If the slight preference for the higher isotopic ratios proved to be real, it would give evidence that the ν process is operating to contribute ^{11}B . On the other hand, if a blending line is present, and $^{11}\text{B}/^{10}\text{B}$ were as low as ~ 1 , this would be inconsistent with pure GCR, and the predictions of VCFO and RLKR, and thus would challenge the current theoretical picture. Observations of one of the recently discovered

B-poor halo stars (Primas *et al.* 1998) would decide between the analyses with and without a blending line presented here, and a more definitive test of the theoretical models.

We wish to thank Lew Hobbs for many helpful discussions. We remember our friend and colleague David Schramm, and acknowledge his support and his comments on the initial manuscript. This research was based on observations obtained with the NASA/ESA *Hubble Space Telescope* through the Space Telescope Science Institute, which is operated by the Association of Universities for Research in Astronomy, Inc., under NASA contract NAS5-26555. This research has made use of NASA’s Astrophysics Data System Abstract Service.

REFERENCES

- Bloemen, H., Wijnands, R., Bennett, K., Diehl, R., Hermsen, W., Lichti, G., Morris, D., Ryan, J., Schönfelder, V., Strong, A. W., Swanenburg, B. N., de Vries, C., & Winkler, C. 1994, *A&A*, 281, L5
- Chaussidon, M. & Robert, F. 1995, *Nature*, 374, 337
- Copi, C., Schramm, D., & Turner, M. 1995, *Science*, 267, 192
- Duncan, D.K., Primas, F., Rebull, L.M., Boesgaard, A.M., Deliyannis, C.P., Hobbs, L.M., King, J.R., & Ryan, S. 1997, *ApJ*, 488, 338
- Duncan, D.K., Rebull, L.M., Primas, F., Boesgaard, A.M., Deliyannis, C.P., Hobbs, L.M., King, J.R., & Ryan, S. 1998, *A&A*, in press
- Edlén, B., Ölme, A., Herzberg, G., & Johns, J.W.C. *J. Opt. Soc. Am.*, 60, 889
- Gray, D.F. 1992 *The Observation and Analysis of Stellar Photospheres*, 2nd edition, Cambridge University Press, p. 407.
- Hobbs, L.M., & Thorburn, J.A. 1994, *ApJ*, 428, L25
- Johansson, S.G., Litzen, U., Kasten, J., and Kock, M. 1993, *ApJ*, 403, L25
- Kiselman, D. & Carlsson, M., 1996, *A&A*, 311, 680
- Kurucz, R. L. 1993, CD-ROM # 1,13,18
- Lambert, D.L., Sheffer, Y., Federman, S.R., Cardelli, J.A., Sofia, U.J., and Knauth, D.C. 1998, *ApJ*, 494, 614
- Lemke, M., Lambert, D.L., & Edvardsson, B., 1993, *PASP*, 105, 468
- Magain, P. 1989, *A&A*, 286, 169
- Meneguzzi, M., Audouze, J., & Reeves, H. 1971, *A&A*, 15, 337
- Morton, D.C. 1991, *ApJS*, 77, 119

Murphy, R.J., Share, G.H., Grove, J.E., Johnson, W.N., Kurfess, J.D., Purcell, W.R., McNaron-Brown, K., & Ramaty, R. 1996, *ApJ*, 473, 990

Nissen, P.E., Lambert, D.L., & Smith, V.V. 1994, *The ESO Messenger*, 76, 36

Primas, F., *et al.* 1998, in preparation.

Ramaty, R., Kozlovsky, B., Lingenfelter, R.E., & Reeves, H. 1997, *ApJ*, 488, 730 (RKLR)

Reader, J., Aquista, N., Sansonetti, C.J., and Sansonetti, J. 1990, *ApJS*, 72, 831

Vangioni-Flam, E., Cassé, M., Fields, B. D., & Olive, K. A. 1996, *ApJ*, 468, 199 (VCFO)

Wagman, N.E., 1937, *Bull. Univ. Pittsburgh* 34, 1, 9

Wagoner, Fowler, & Hoyle, F.

Walker, T.P., Steigman, G., Schramm, D.N., Olive, K.A., & Fields, B. 1993, *ApJ*, 413, 562

Woosley, S.E., Hartmann, D.H., Hoffman, R.D., & Haxton, W.C. 1990, *ApJ*, 356, 272

Table 1: Boron line parameters, including $\log gf$ values for varying isotopic ratios, from Johansson *et al.* (1993).

isotope	λ	gf	$\log gf$ for 1:1	$\log gf$ for 2.5:1	$\log gf$ for 4:1	$\log gf$ for 10:1
10	208.95898	0.170	-1.0706	-1.167	-1.372	-1.770
11	208.95650		-1.0706	-0.991	-0.894	-0.815
10	208.89084	0.095	-1.3233	-1.420	-1.624	-2.022
11	208.88835		-1.3233	-1.244	-1.147	-1.068
10	208.95760	0.019	-2.0223	-2.119	-2.323	-2.721
11	208.95510		-2.0233	-1.943	-1.846	-1.767

Table 2: LiBeB production (based on VCFO).

source	${}^6\text{Li}$	${}^7\text{Li}$	${}^9\text{Be}$	${}^{10}\text{B}$	${}^{11}\text{B}$	${}^{11}\text{B}/{}^{10}\text{B}$
GCR	yes	yes	yes	yes	yes	2.5
ν process	no	yes	no	no	yes	large, if full yields are used.
LECR	yes	yes	yes	yes	yes	ranges, 3-5

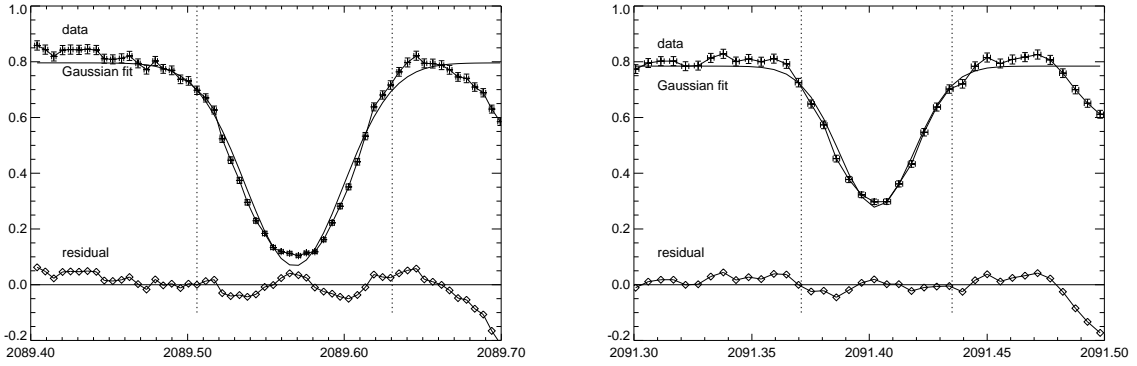


Fig. 1.— Symmetry of the B line (a) and a narrow stellar line at $\lambda 2091.4$ (b): comparison of a Gaussian to the lines. Residuals are shown in the lower panel of each Figure. Conventions (dotted vertical lines and data point symbols) are explained in the text.

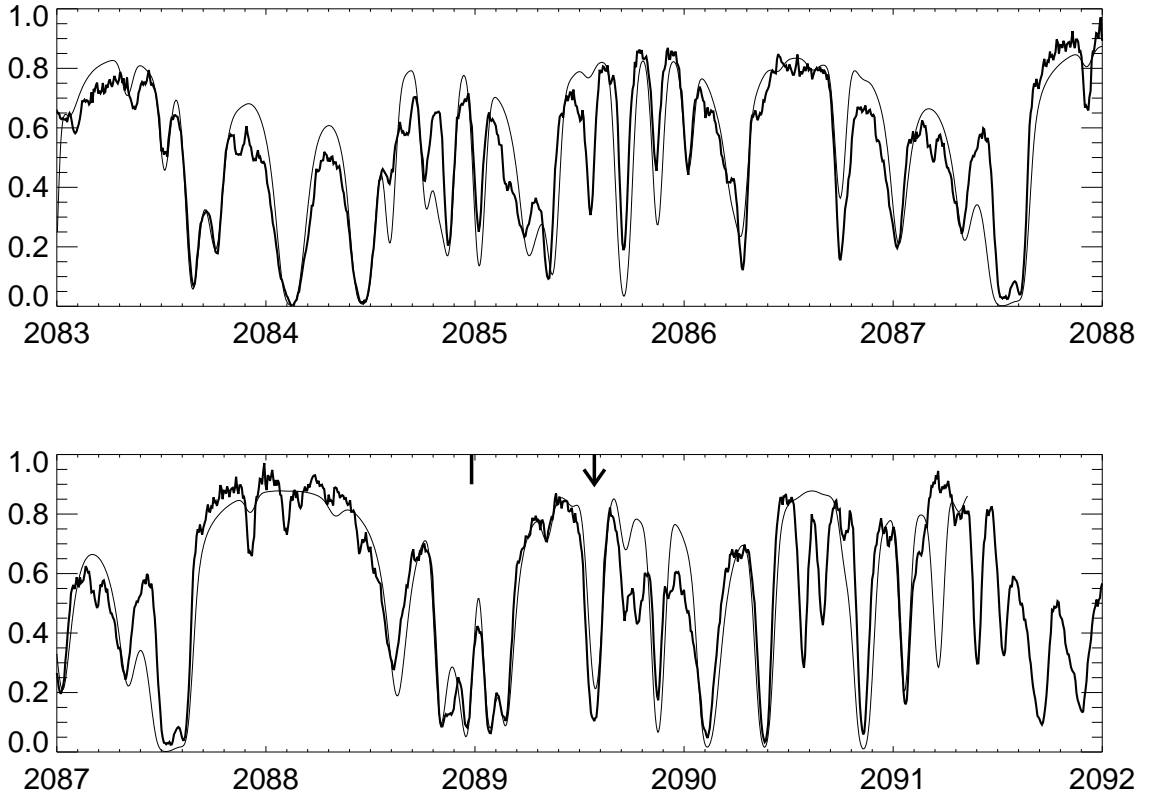


Fig. 2.— Plot of HD 76932 data (thick) and Kurucz synthesis (thin). Net broadening is 4.7 km/s, total boron abundance is 1.82 dex, and isotope ratio is 1:1. The boron line of interest is marked at 2089.571 Å.

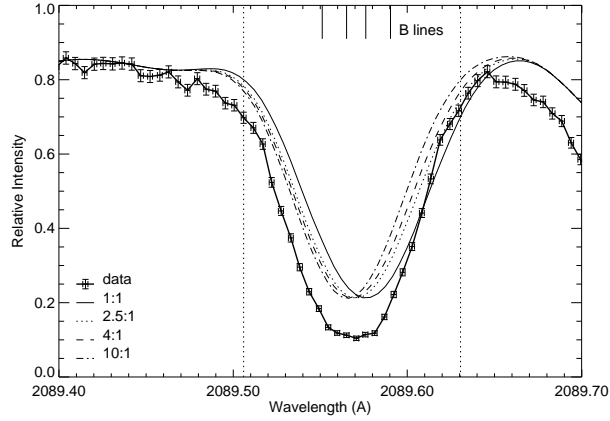


Fig. 3.— Plot of B line and syntheses with total $\log \epsilon(\text{B})=1.82$, at isotopic ratios of 1:1, 2.5:1, 4:1, and 10:1. The locations of the B lines are indicated; vertical dotted lines are as in previous figures.

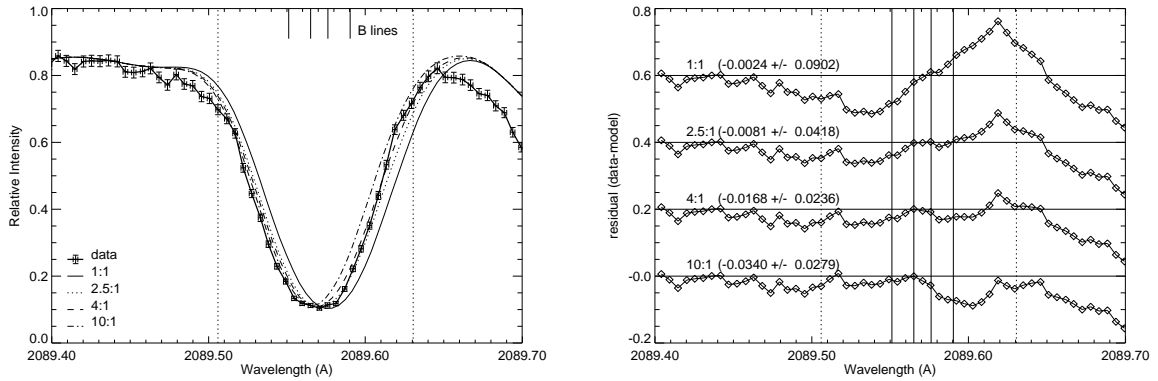


Fig. 4.— B line and syntheses (a) and residuals (b) for total $\log \epsilon(\text{B})=2.07$, at isotopic ratios of 1:1, 2.5:1, 4:1, and 10:1. Notation is as in previous figures. Mean and standard deviation of residuals from the fit are given for each plot in (b).

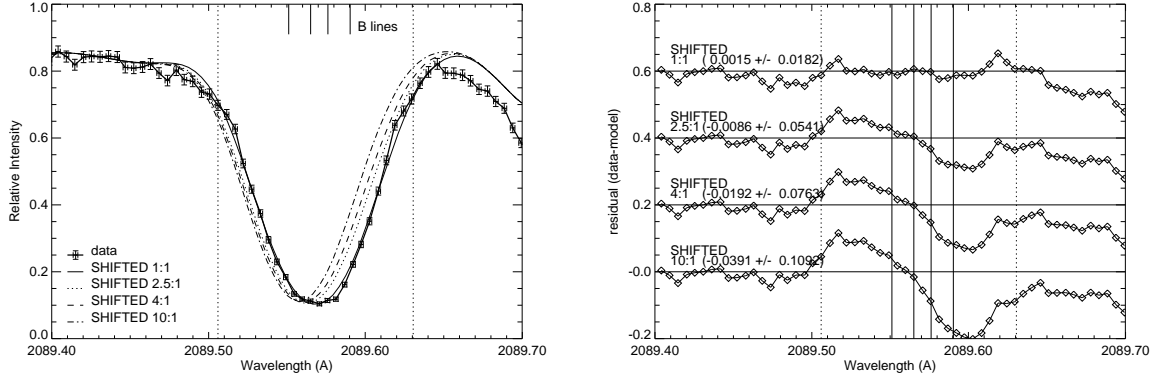


Fig. 5.— Plot of B line and syntheses (a) and residuals (b) for total $\log \epsilon(B)=2.07$, at all four isotopic ratios as before; but with the syntheses are shifted 0.007 \AA to the blue, which does NOT provide a good match to the rest of the spectrum. Notation is as in previous figures.

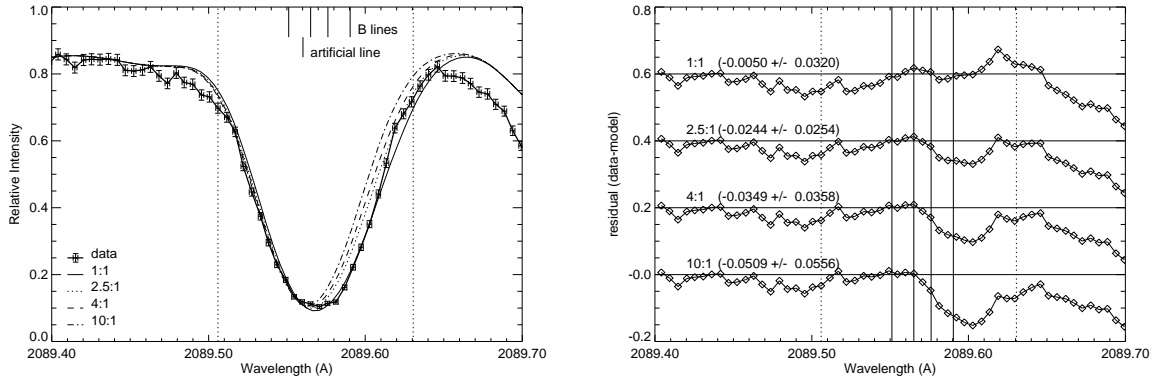


Fig. 6.— Plot of B line and syntheses (a) and residuals (b) for an artificial blending line at 2089.560 \AA , total $\log \epsilon(B)=1.82$. Notation is as in previous figures.

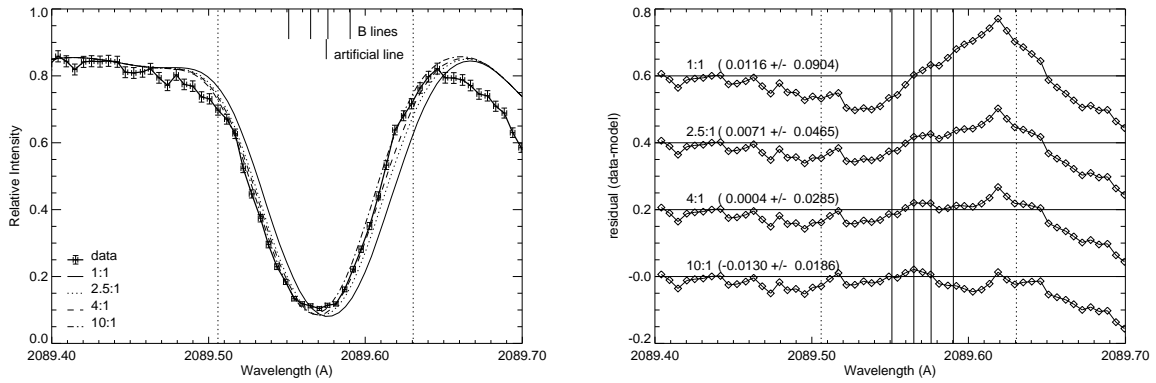


Fig. 7.— Same as Figure 6, but with the artificial blending line at 2089.575 \AA , total $\log \epsilon(\text{B})=2.07$. Notation is as in previous figures.

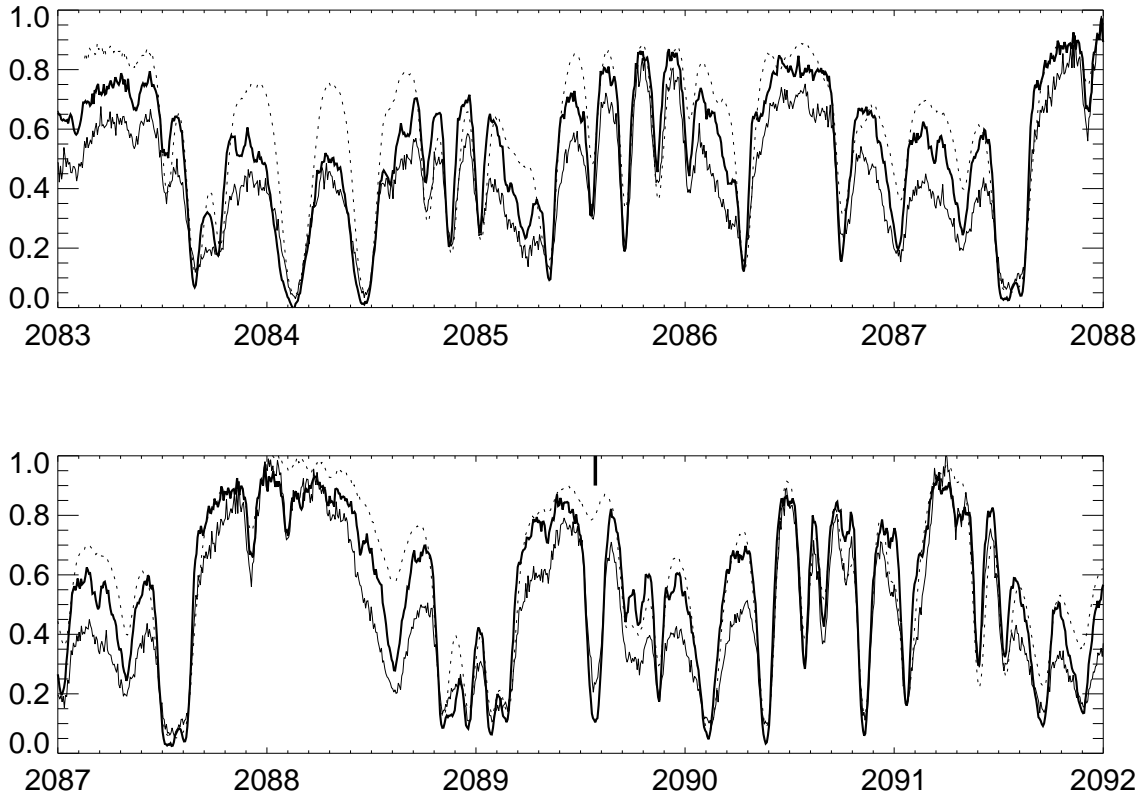


Fig. 8.— Comparison of HD 76932 (thick), HD 102870 (thin), and HD 61421 (dotted). The location of the B lines is indicated. Note that the data have been normalized to each other, and are not necessarily properly normalized for comparison to a metal-rich synthesis.